Application Note

Cell Migration and Invasion

Agilent
Trusted Answers

# Advanced Wound Healing Assay Workflow using Automated Scratch Wound Creation, High Contrast Brightfield and Fluorescence Kinetic Imaging


**Author**

Brad Larson
Agilent Technologies, Inc.



## Abstract

Multiple components, including extracellular matrix and stromal cells, play a role in constructing *in vivo* tissues or cancer cell models. When performing scratch wound healing assays to determine the migratory patterns of target cell types included in these models, it is important to create the most *in vivo*-like setting for pre-clinical *in vitro* tests. The current standard for performing scratch wound assays involves manual wounding of a cell layer created on the bottom of a noncoated plate, and label-free cellular analysis. With the addition of an automated wound creation method, in addition to kinetic image capture and analysis of both brightfield and fluorescent signals from single and co-cultured cells, robust data can be generated to allow accurate assessments of potential promotion of wound closure or prevention of metastatic cell migration.

## Introduction

Several components of the tumor microenvironment are known to contribute to *in vivo* disease progression and metastatic behavior. The extracellular matrix (ECM) is one such contributing factor. The ECM is a complex cellular scaffold found throughout the body that consists of collagen, cell-adhesive glycoproteins and other proteins. ECM supports adhesion and intracellular communication networks, and also facilitates cellular migration, including directionality, as a collective group.[1] This type of migration is a significant aspect of wound healing and also of tumor metastasis, which is the primary cause of cancer morbidity and mortality.[2] Additionally, stromal cells, such as fibroblasts, are found within *in vivo* cellular models commonly studied using *in vitro* scratch wound healing methodologies. Fibroblasts are responsible for depositing components of the ECM, and in the solid tumor microenvironment, influence cancer cells in migration, invasion and other tumorigenic processes.[3] The presence of these cells is widespread among cancers such as pancreatic, lung, and head and neck squamous cell carcinoma (HNSCC).[4-6] Because of the important role that ECM and stroma play *in vivo*, each should be included when performing *in vitro* cell migration studies to increase the relevance of generated data.

The wound healing or scratch assay is a straightforward and widely used method to measure cell migration. In the method, once cultured cells reach confluence, the monolayer is mechanically scratched, thus creating a cell-free zone, and for some cell models simulates a wound area. Collective cell migration into the cell-free zone is then kinetically imaged over time to characterize cell movement when uninhibited or under the influence of a test molecule. When wounds are created manually, most times using a pipette tip, the wound width, orientation and placement within the well are difficult to standardize.[7] Without reproducibility, variability in calculated measurements within replicate wells and across titrations can complicate final conclusions regarding cell migratory behaviors.

Here we demonstrate the use of a novel, automated tool to create consistent and reproducible scratch wounds in cell monolayers formed on the bottom of a microplate well. We use a single cancer cell model as well as a co-culture of fibroblasts and cancer cells; each plated in collagen-coated microplate wells to more closely simulate *in vivo* microenvironments and facilitate cell migration. The tool fits into any size laminar flow hood and features an interchangeable pin manifold for use with 24- or 96-well plates, as well as a preprogrammed, hands-free cleaning and decontamination protocol to reduce the risk of contamination. Following scratch wound generation, the plate is transferred to an Agilent BioTek automated imager or the Agilent BioTek BioSpa live cell imaging system to kinetically monitor cell migration using high contrast brightfield and fluorescence imaging.

## Materials and methods

### Materials

**Cells**: HT-1080 fibrosarcoma cells (part number CCL-121) were purchased from ATCC (Manassas, VA). Human neonatal dermal fibroblasts expressing RFP (part number cAP-0008RFP) were purchased from Angio-Proteomie (Boston, MA). U-87 glioblastoma cells expressing GFP were generously donated by Dr. Sachin Katyal (University of Manitoba, Winnipeg, Manitoba, Canada).

**Experimental components:** Advanced DMEM (part number 12491-015), fetal bovine serum (part number 10437-036), penicillin-streptomycin-glutamine (100x) (part number 10378-016), TrypLE express enzyme (1x), phenol red (part number 12605-010), Alconox powdered precision cleaner (part number 16-000-104), and Virkon-S (part number NC9821357) were purchased from ThermoFisher Scientific (Waltham, MA). Collagen Type I, Bovine (FITC) (part number C7510-11) was purchased from US Biological (Salem MA). Acetic acid (part number A6283) was purchased from Millipore Sigma. 24-well clear TC-treated multiple well plates (part number 3524) and 96-well clear, flat bottom, polystyrene TC-treated microplates (part number 3598) were purchased from Corning Life Sciences (Corning, NY).


**Agilent BioTek AutoScratch wound making tool:** The AutoScratch wound making tool automatically creates reproducible scratch wounds in cell monolayers grown in microplates. The simple pushbutton operation and tool-free scratch pin manifold exchange make it easy to process either 96- or 24-well plates, which are commonly used in migration and invasion assays. The compact system features an onboard, preprogrammed cleaning routine to keep the scratch pins free of cell buildup and avoid contamination. AutoScratch precisely and efficiently automates the sample prep for imaging workflows with Agilent BioTek Cytation cell imaging multimode readers and Agilent BioTek Lionheart automated microscopes.

**Agilent BioTek Cytation 5 cell imaging multimode reader:** Cytation 5 is a modular multimode microplate reader combined with an automated digital microscope. Filter- and monochromator-based microplate reading are available, and the microscopy module provides up to 60x magnification in fluorescence, brightfield, color brightfield and phase contrast. The instrument can perform fluorescence imaging in up to four channels in a single step. With special emphasis on live-cell assays, Cytation 5 features shaking, temperature control to 65 °C, $CO_2/O_2$ gas control and dual injectors for kinetic assays and is controlled by integrated Agilent BioTek Gen5 microplate reader and imager software, which also automates image capture, analysis and processing. The instrument was used to kinetically monitor cell migration using either high contrast brightfield or fluorescence imaging channels.

**Agilent BioTek BioSpa 8 automated incubator:** The BioSpa 8 automated incubator links Agilent BioTek readers or imagers together with Agilent BioTek washers and dispensers for full workflow automation of up to eight microplates. Temperature, $CO_2/O_2$ and humidity levels are controlled and monitored through the Agilent BioTek BioSpa software to maintain an ideal environment for cell cultures during all experimental stages. Test plates were incubated in the BioSpa to maintain proper atmospheric conditions for appropriate times optimized with each tested cell model and automatically transferred to the Cytation 5 for brightfield and fluorescence imaging.

**Agilent BioTek MultiFlo FX multimode dispenser:** The MultiFlo FX is a modular, upgradable reagent dispenser with as many as two peri-pump (8 tube dispensers), two syringe pump dispensers and a strip washer. The syringe and washer manifolds can be configured for plate densities from 6- to 384-well.

## Methods

**Collagen plate coating:** A 0.02 M concentration of acetic acid was used to dilute the collagen 1:30, for a final concentration of 33 µM. A 50 µL volume of the diluted collagen was added to each well of 96-well test plates, while a 300 µL volume was added to each well of 24-well test plates. Plates were left open in a sterile environment to allow liquid evaporation and collagen coating of the wells.

**Cell preparation:** Cells were cultured in T-75 flasks until reaching 80% confluence. Subsequent to detachment from the flask with TrypLE, cells were resuspended to pre-optimized concentrations depending on plate well density and culture conditions (Table 1). Diluted cells, in a volume of 100 µL for 96-well plates or 1 mL for 24-well plates, were then added to test plates.

**Table 1.** Cell model 24- and 96-well plating concentrations.

| Cell Plating Concentrations | | |
|---|---|---|
| | **24-Well Format** | **96-Well Format** |
| HT-1080 | $2.4 \times 10^5$ cells/mL | $4.0 \times 10^5$ cells/mL |
| Fibroblast | - | $2.0 \times 10^5$ cells/mL |
| U-87 | $2.4 \times 10^5$ cells/mL | - |
| Fibroblast/U-87 Co-culture | - | $3.0 \times 10^5$ cells/mL/$3.0 \times 10^5$ cells/mL |

**AutoScratch cleaning procedure:** Prior to wound creation in test plates, the AutoScratch tool pins were cleaned and sterilized. The four cleaning components were added to individual reservoirs of the cleaning trough and labeled to assist with appropriate component and volume addition (Table 2). Final Alconox and Virkon-S solutions were previously prepared using procedures described by the vendor.

**Table 2.** Cleaning trough reagent setup.

| AutoScratch Cleaning Components | | |
|---|---|---|
| Reservoir #1 | Alconox, 0.5% | 12 mL |
| Reservoir #2 | Virkon-S, 1% | 12 mL |
| Reservoir #3 | Sterile DI $H_2O$ | 12 mL |
| Reservoir #4 | 70% Ethanol | 12 mL |

The cleaning procedure was initiated. During the process, the scratching arm containing the pins moved from the home position into the reservoir containing 0.5% Alconox, agitated in the Y-axis for three seconds, then soaked the pins in the component for five minutes. At the completion of the five-minute incubation period, the arm moved the pins to the Virkon-S. The process was then automatically repeated for each of the remaining components. At the end of the twenty-minute cleaning cycle, the pins were clean, sterile, and ready to be used for wound creation.

**Scratch wound creation:** Following completion of the cleaning procedure, the test plate was added to the AutoScratch tool deck and the lid removed. The **Scratch** button appropriate for the microplate density being used, **24** or **96**, was pressed to begin the wounding process. The arm moved the pins from the home position to column 1 of the plate where a scratch was made vertically at the center of the well. The arm then moved the pins back to the reservoir containing the DI $H_2O$ and performed a three second agitation to remove any dislodged cells on the pins. The pins were then automatically moved to column 2 and the scratching and cleaning steps were repeated for each column of the plate.

**Post scratch plate washing:** Upon completion of the wound creation routine, the plate was transferred to a separate laminar flow hood containing the MultiFlo FX, and a plate washing procedure was carried out to remove cells dislodged from the bottom of the plate. Stainless steel tubes of the strip washer, previously sterilized using 70% ethanol, were used to aspirate media while the peristaltic pump and an autoclaved 5 µL cassette dispensed fresh media. For uninhibited wells, the procedure was repeated three times. For wells containing the cytochalasin D titration, media containing inhibitor was added manually following the third aspiration cycle.

**Kinetic image-based monitoring of cell migration:** Plates were then placed into the BioSpa 8, with atmospheric conditions previously set to 37 °C/5% $CO_2$. Water was added to the pan to create a humidified environment. The BioSpa 8 software was programmed such that the plates were automatically transferred to Cytation 5 for high contrast brightfield or high contrast brightfield and fluorescent imaging of the test wells, depending on the incorporated cell types. A single 4x image was taken with each channel (Table 3) to capture potential cell movement into the original wound area.

**Table 3.** Included imaging channels per test cell model.

| Incorporated Imaging Channels | |
|---|---|
| HT-1080 | High contrast brightfield |
| Fibroblast | High contrast brightfield/RFP |
| U-87 | High contrast brightfield/GFP |
| Fibroblast/U-87 Co-culture | High contrast brightfield/RFP/GFP |

Plates were then transferred back to the BioSpa 8. Kinetic imaging cycles were carried out using iterations optimized depending on the speed of migration for each cell model (Table 4).

**Table 4.** Optimized imaging intervals per cell model.

| Kinetic Imaging Intervals | |
|---|---|
| HT-1080 | 60 minutes |
| Fibroblast | 90 minutes |
| U-87 | 90 minutes |
| Fibroblast/U-87 Co-culture | 90 minutes |

**Image processing:** Following capture, using the settings in Table 5, high contrast brightfield images were processed to increase the contrast in brightfield signal between background and cell containing areas of the image, while fluorescent images were processed to remove background signal.

**Table 5.** Image preprocessing parameters.

| Image Preprocessing Parameters | | | | |
|---|---|---|---|---|
| **Channel** | **Apply Image Processing** | **Background** | **Rolling Ball Diameter** | **Priority** |
| High contrast brightfield | Yes | Dark | 25 µm | Fine results |
| RFP | Yes | Dark | 500 µm | Fine results |
| GFP | Yes | Dark | 500 µm | Fine results |

**Cellular analysis of preprocessed images:** Cellular analysis was carried out on the processed images to quantify the cell containing areas of each image. For HT-1080 cells, the high contrast brightfield channel was used, along with the criteria in Table 6.

**Table 6.** High contrast brightfield-based object mask analysis parameters for HT-1080 cells.

| High Contrast Brightfield Primary Cellular Analysis Parameters: HT-1080 Cell Model | |
|---|---|
| Channel | Tsf[Brightfield] |
| Threshold | 2,000 |
| Background | Dark |
| Split Touching Objects | Unchecked |
| Fill Holes in Masks | Checked |
| Minimum Object Size | 100 µm |
| Maximum Object Size | 10,000 µm |
| Include Primary Edge Objects | Checked |
| Analyze Entire Image | Checked |
| **Advanced Detection Options** | |
| Rolling Ball Diameter | 40 |
| Image Smoothing Strength | 20 |
| Evaluate Background On | 1% of lowest pixels |
| Expand the Threshold Mask | 5 µm |
| **Analysis Metric** | |
| Metric of Interest | Object sum area |

For RFP expressing fibroblasts and GFP expressing U-87 cells, the high contrast brightfield channel was again used, along with the criteria in Table 7.

**Table 7.** High contrast brightfield-based object mask analysis parameters for U-87 and fibroblast cells.

| High Contrast Brightfield Primary Cellular Analysis Parameters: U-87 and Fibroblast Cell Models | | |
|---|---|---|
| | **Fibroblast** | **U-87** |
| Channel | Tsf[Brightfield] | Tsf[Brightfield] |
| Threshold | 850 | 1700 |
| Background | Dark | Dark |
| Split Touching Objects | Unchecked | Unchecked |
| Fill Holes in Masks | Unchecked | Unchecked |
| Min. Object Size | 10 µm | 10 µm |
| Max. Object Size | 10,000 µm | 10,000 µm |
| Include Primary Edge Objects | Checked | Checked |
| Analyze Entire Image | Checked | Checked |
| **Advanced Detection Options** | | |
| Rolling Ball Diameter | 50 | 50 |
| Image Smoothing Strength | 5 | 5 |
| Evaluate Background On | 1% of lowest pixels | 1% of lowest pixels |
| **Analysis Metric** | | |
| Metric of Interest | Object sum area | Object sum area |

However, as these cells also express a fluorescent signal, captured RFP or GFP images were also used to perform separate analyses in addition to the criteria described in Table 8.

**Table 8.** Fluorescence-based object mask analysis parameters.

| Fluorescence Primary Cellular Analysis Parameters: U-87 and Fibroblast Cell Models | | |
|---|---|---|
| | **Fibroblast** | **U-87** |
| Channel | Tsf[RFP] | Tsf[GFP] |
| Threshold | 250 | 300 |
| Background | Dark | Dark |
| Split Touching Objects | Unchecked | Unchecked |
| Fill Holes in Masks | Unchecked | Unchecked |
| Minimum Object Size | 50 µm | 10 µm |
| Maximum Object Size | 10,000 µm | 10,000 µm |
| Include Primary Edge Objects | Checked | Checked |
| Analyze Entire Image | Checked | Checked |
| **Advanced Detection Options** | | |
| Rolling Ball Diameter | 50 | 50 |
| Image Smoothing Strength | 20 | 20 |
| Evaluate Background On | 5% of lowest pixels | 5% of lowest pixels |
| **Analysis Metric** | | |
| Metric of Interest | Object sum area | Object sum area |

**Wound healing metric calculation:** The kinetic cell area coverage values (Object Sum Area) were then used to generate three additional wound healing metrics including wound width, wound confluence, and maximum wound healing rate. Each metric was automatically calculated by the Gen5 wound healing protocol.

### Wound width

Wound width, or the average width of the cell free zone over time, was calculated using the following formula:

$$W_t = \frac{I_A - \text{Object Sum Area}_t}{I_H}$$

Where $W_t$ is the average wound width (µm) over time, $I_A$ is the total area of the 4x image, Object Sum $\text{Area}_t$ is the area covered by cells at each time point, and $I_H$ is the height of a 4x image.

### Wound confluence

Wound confluence, or the percentage of the original wound area covered by migrating cells over time, was calculated using the following formula:

$$C_t = \frac{(\text{Object Sum Area}_t - \text{Object Sum Area}_0) \times 100}{I_A - \text{Object Sum Area}_0}$$

Where $C_t$ is the percent wound confluence over time, Object Sum $\text{Area}_t$ is the area covered by cells at each time point, Object Sum $\text{Area}_0$ is the area covered by cells at time 0, and $I_A$ is the total area of the 4x image.

### Maximum wound healing rate

The maximum wound healing rate was calculated using a Kinetic Analysis step in Gen5 software. The Max V calculation type was selected and the rate was calculated using six data points along the sum area curve. The value was then expressed as $\mu m^2$ per hour.

## Results and discussion

### Scratch wound creation within collagen coated plates

An increasing number of publications have shown that extracellular matrix-coated wells, which cells then attach to and interact with, create a more *in vivo*-like environment when performing *in vitro* experimental procedures. Therefore, experiments were carried out with the AutoScratch unit to evaluate its ability to consistently create wounds in cell layers attached to wells previously coated with a collagen ECM. To perform this assessment, HT-1080 cells were plated into each well of 96- or 24-well microplates using volumes previously described and concentrations explained in Table 1. Following an overnight incubation to allow for attachment, the plates were placed one at a time onto the deck and scratched by the AutoScratch tool to create wounds in each well. Visual inspection of high contrast brightfield images from each plate type, as shown in Figure 1A and B, illustrated consistent wounds of similar shape and size to those created in non-collagen coated plates (Figure 1C).

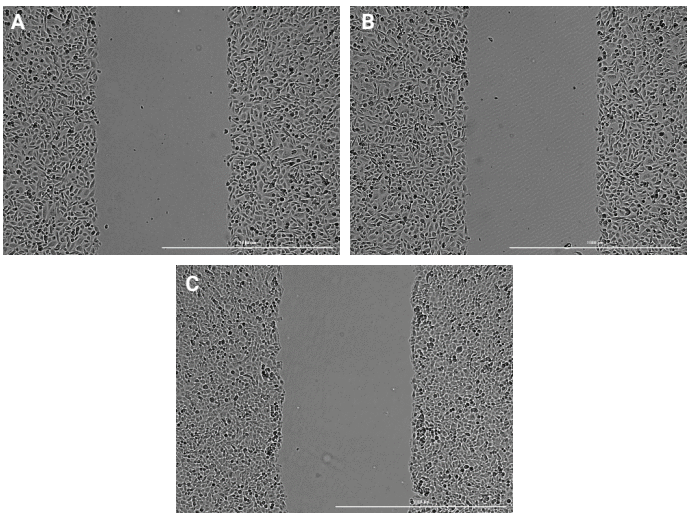


**Figure 1.** Test plate image capture. High contrast brightfield images, 4x, captured from collagen coated (A) 96-; and (B) 24-well plates, in addition to (C) 96-well non-collagen coated plates immediately following wound creation with AutoScratch.

To quantify the consistency of wound creation, high contrast brightfield images (Figure 2A) were preprocessed using the parameters described in Table 5. Using this method, the contrast between image areas containing cells and background is increased (Figure 2B). This allows accurate object mask placement around cell containing areas (Figure 2C) using the cellular analysis criteria in Table 6.

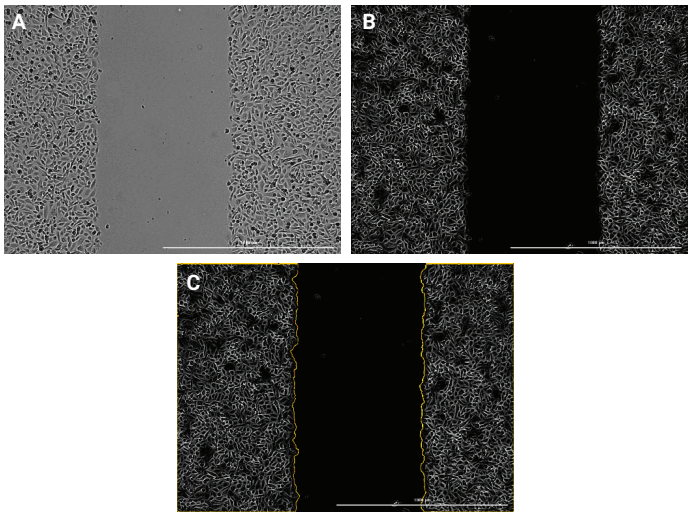


**Figure 2.** High contrast brightfield image processing and analysis. (A) Raw high contrast brightfield image; (B) preprocessed high contrast brightfield image; and (C) preprocessed high contrast brightfield image with object mask placement.

Using the wound width formula described previously, the average wound width at time 0 following wound creation was generated for each well of the 96- and 24-well plates. The %CV of wound width values across all wells of the collagen coated 96-well test plate was 1.8%, whereas the %CV of the wound width values across the collagen coated 24-well test plate was 1.5%. When comparing these values to those generated using non-collagen coated plates, 2.1% in 96-well format and 1.4% in 24-well format, it is clear that a high degree of repeatability in wound size was achieved when using the AutoScratch tool with uncoated plates or those containing an ECM in either plate well density.

While wound creation was equivalent and independent of the presence or lack of an ECM layer, an interesting phenomenon was observed when uninhibited cell migration was allowed to proceed. Per Figure 3, HT-1080 cells plated on collagen achieved complete wound closure in approximately 4.5 hours with a maximum wound healing rate of $2.5 \times 10^5$ $\mu m^2$/hour, while HT-1080 cells plated on noncoated wells achieved complete wound closure in approximately 6.5 hours with a maximum wound healing rate of $2.0 \times 10^5$ $\mu m^2$/hour.

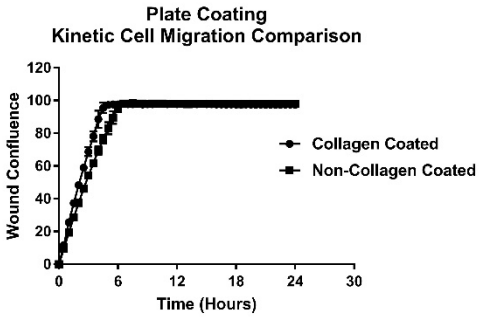


**Figure 3.** Average plus/minus standard deviation plotted from uninhibited wells containing HT-1080 cells plated on collagen coated, or non-collagen coated surfaces.

## Combining high contrast brightfield and fluorescence to generate kinetic wound healing metrics

In order to examine the unique migratory pattern of cell types included in a co-culture model, cells expressing a separate fluorescent protein or labeled with a different fluorescent probe are commonly incorporated. This allows for the monitoring of individual cell types using separate fluorescence channels (Figure 4).

Wound healing tests were performed with two separate cell types expressing fluorescent proteins, U-87 GFP and primary fibroblast RFP, to validate whether performing cellular analysis on migrating cells using fluorescence provided equivalent data to that generated using the high contrast brightfield signal. U-87 cells were plated in a 24-well plate, while fibroblasts were plated in a 96-well plate using the cell concentrations explained in Table 1. Following wound creation with the AutoScratch and washing, cells in each well were allowed to migrate uninhibited back into the cell free zone. Cellular analysis was performed using high contrast brightfield and either GFP for U-87 cells or RFP for fibroblasts. Kinetic wound confluence curves were then plotted for each analysis method (Figure 5).

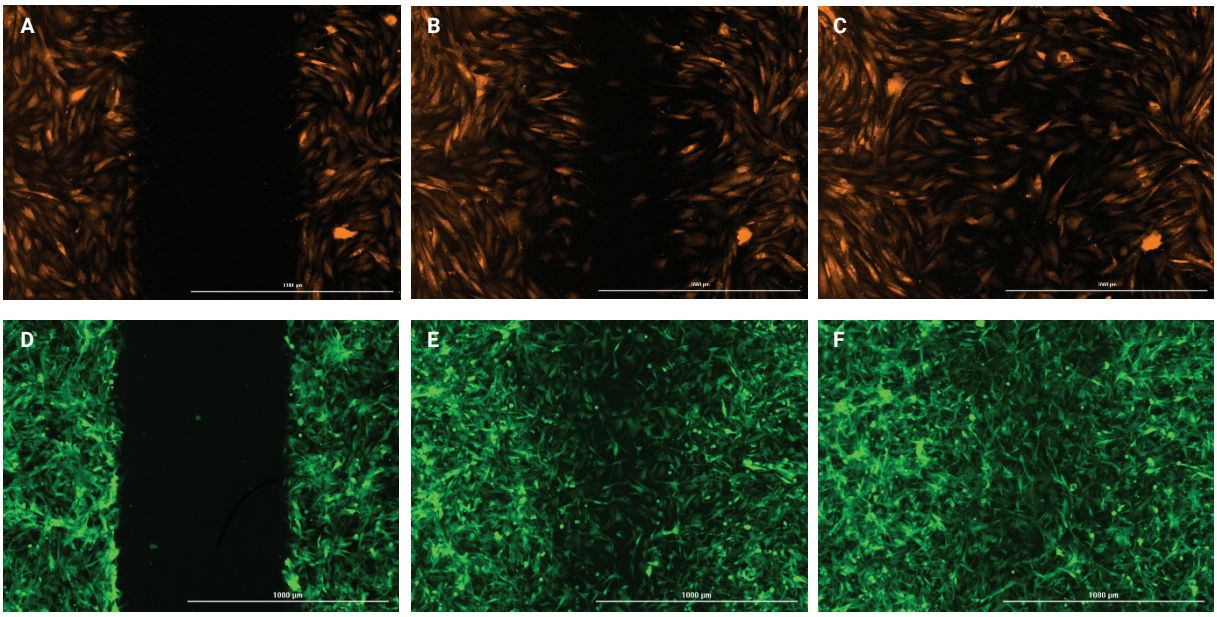


**Figure 4.** Fluorescent images of fibroblast and U-87 wound healing. Kinetic images captured of uninhibited RFP expressing fibroblast cell migration after (A) 0, (B) 10, and (C) 24 hour incubations; and GFP expressing U-87 cell migration after (D) 0, (E) 10, and (F) 24 hour incubations. Cells plated in wells previously coated with collagen I.

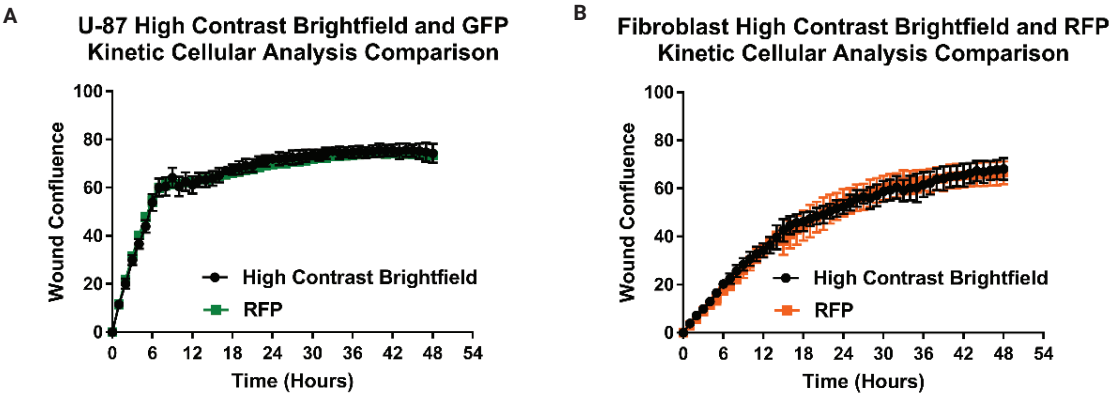


**Figure 5.** Average kinetic U-87 and fibroblast wound confluence graphs. Average, plus/minus standard deviation plotted at every captured timepoint using high contrast brightfield and fluorescence-based analysis for uninhibited (A) 24-well plated U-87 cells; and (B) 96-well plated fibroblasts.

The similarity of the kinetic wound confluence curves generated using either high contrast brightfield or fluorescent signals for U-87 cells (Figure 5A), or fibroblasts (Figure 5B), in addition to the correlation between the average maximum wound healing rates (Table 9), at 95% confidence intervals for both cell types, confirm that analysis with high contrast brightfield or fluorescence yield equivalent results.

**Table 9.** Maximum wound healing rates using high contrast brightfield or fluorescent signals for U-87 and fibroblast cell models.

| U-87 and Fibroblast Maximum Wound Healing Rates | | |
|---|---|---|
| | High Contrast Brightfield | Fluorescence |
| U-87 | Avg: 9.7x10⁴ µm²/hour/%CV: 1.1% | Avg: 9.7x10⁴ µm²/hour/%CV: 2.0% |
| Fibroblast | Avg: 6.1x10⁴ µm²/hour/%CV: 2.7% | Avg: 6.1x10⁴ µm²/hour/%CV: 3.1% |

## Use of co-cultured cell models

To illustrate the use of the AutoScratch and Gen5 cellular analysis with a more *in vivo*-like cell model, including cancerous and stromal cell types, GFP expressing U-87 glioblastoma cells and RFP expressing primary fibroblasts were added to the wells of a 96-well plate at concentrations listed in Table 1. Following wound creation and washing, an 8-point titration of cytochalasin D, ranging from 10,000 to 2.4 nM using 1:4 serial titrations, including a no compound negative control, was added to four replicates each going down the rows of the plate. Cells were then allowed to migrate uninhibited or in the presence of cytochalasin D for 48 hours (Figure 6).

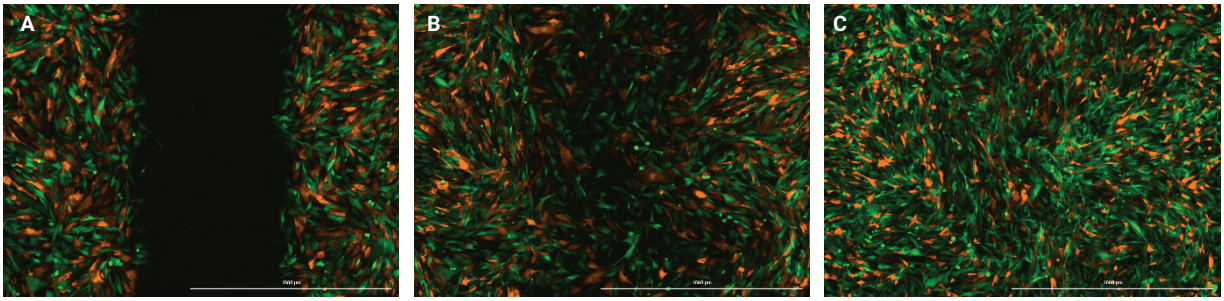


**Figure 6.** Fluorescent images of fibroblast and U-87 co-cultured wound healing. Kinetic images captured of uninhibited RFP expressing fibroblast and GFP expressing U-87 cell migration after (A) 0, (B) 18, and (C) 48 hour incubations.

Cellular analysis was then performed to assess the migration characteristics of each included cell type. However, as neither the fibroblasts or U-87 cells form a confluent monolayer on each side of the created wound, a new analysis method was incorporated.

In the analysis step, an image plug was applied covering the areas to the left and right of the wound created by AutoScratch, leaving only the cell-free zone. In this way only cell migration into the open, uncovered areas of the image was analyzed (Figure 7).

Because of the accuracy in X- and Y-axis coordinates of the AutoScratch created wounds from well to well, the same image plug when applied generated equivalent data between replicate wells for each cell type (Figure 8).

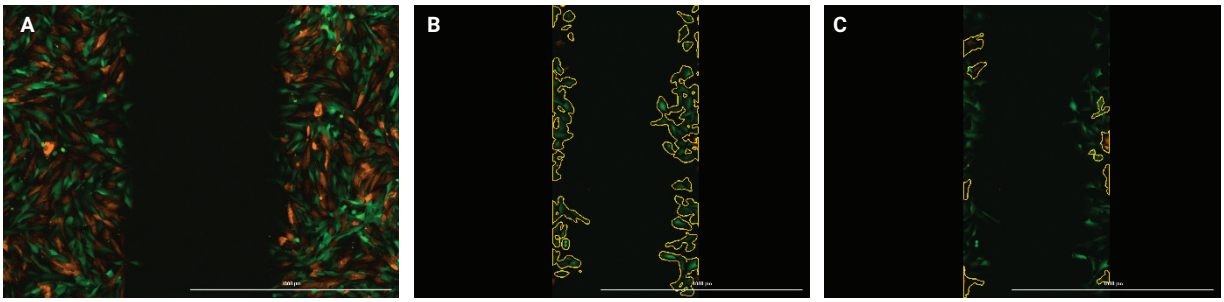


**Figure 7.** Cellular analysis of individual co-cultured cell types within created wound. (A) Overlaid fluorescent images of RFP expressing fibroblasts and GFP expressing U-87 cells immediately following wound creation. (B) Cellular analysis of GFP signal from U-87 cells post 3 hour incubation. (C) Cellular analysis of RFP signal from fibroblasts post 3 hour incubation.

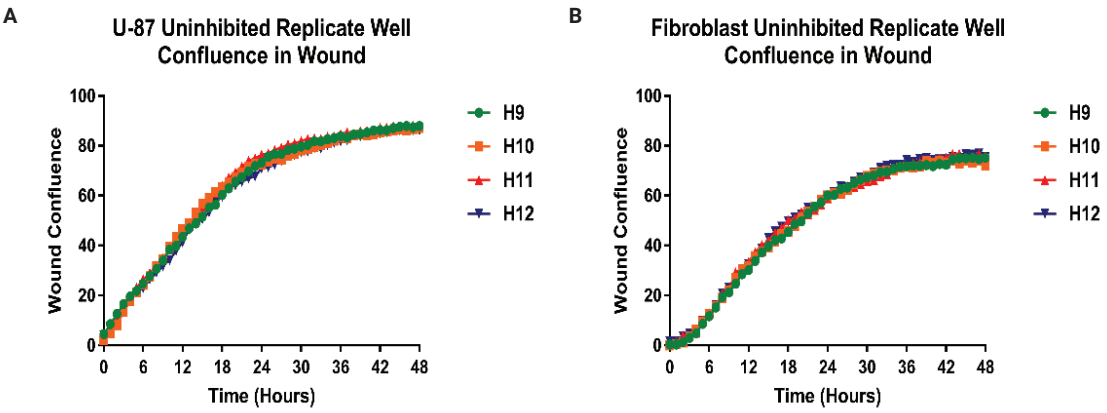


**Figure 8.** Kinetic replicate confluence in created wound curves. (A) Wound confluence curves generated using U-87 GFP signal from four replicate uninhibited wells. (B) Wound confluence curves generated using Fibroblast RFP signal from four replicate uninhibited wells.

Kinetic wound confluence curves were then plotted to ascertain any possible differences between the cell migration patterns of the co-cultured cell models (Figure 9).

When comparing the two kinetic curves for the first six hours following wound creation (Figure 9A), it is clear that the U-87 glioblastoma cells had a higher initial rate of migration compared to the fibroblasts, which demonstrated low migratory rates, particularly in the first four hours. This was confirmed when examining the differences in object mask area coverage following three hours of incubation between U-87 (Figure 7B) and fibroblast (Figure 7C) cells. The migration rates then become equivalent between the two cell types from 4 to 24 hours post wound creation before the fibroblast migration rate again slows compared to the U-87 cells during the final 24 hours of incubation (Figure 9B). By applying the image plug and performing two separate cellular analyses using fluorescent signals, the subtle differences in migratory patterns between co-cultured cell types were able to be identified and scrutinized to determine possible larger meanings for *in vivo* cancer cell metastasis.

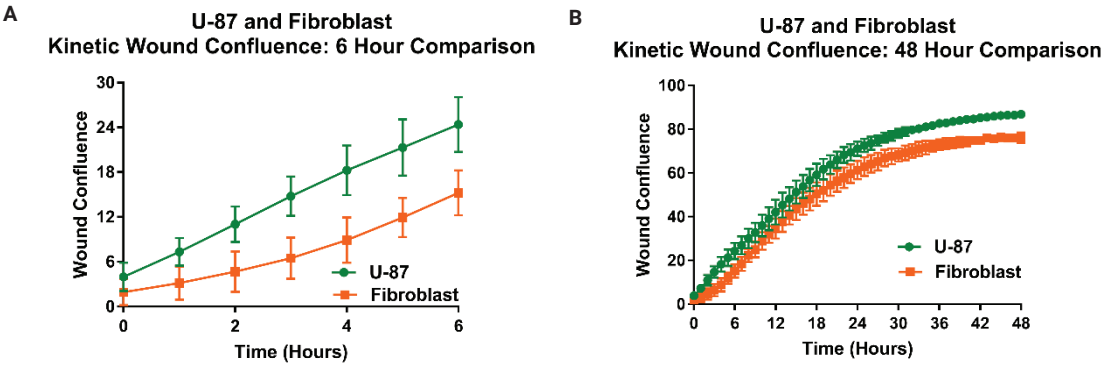


**Figure 9.** Uninhibited cell migration curves of co-cultured cell models. Kinetic wound confluence curves for GFP expressing U-87 cells and RFP expressing fibroblasts. Curves shown for (A) 6 hour; and (B) 48 hour incubations.

## Conclusion

The Agilent BioTek AutoScratch wound making tool has the ability to create consistent wounds in an automated fashion in both 96- and 24-well plates containing an extracellular matrix coating, such as collagen. Validation data proves that the addition of an ECM increases the migratory capability of test cell types, while wound creation does not adversely affect test results. The addition of cellular analysis techniques using fluorescent signals also enables assessment of the migratory ability of individual co-cultured cell types, allowing for the creation and proper evaluation of *in vivo*-like tissue and cancer cell models.

## References


1. Jonkman, J. E.; Cathcart, J. A.; Xu, F.; Bartolini, M. E.; Amon, J. E.; Stevens, K. M.; Colarusso, P. An Introduction to the Wound Healing Assay Using Live-Cell Microscopy. *Cell Adhes. Migr.* **2014**, *8(5)*, 440-451.
2. Seyfried, T. N.; Huysentruyt, L. C. On the Origin of Cancer Metastasis. *Crit. Rev. Oncog.* **2014**, *18(1-2)*, 43-73.
3. Rajaram, M.; Li, J.; Egeblad, M.; Powers, R. S. System-Wide Analysis Reveals a Complex Network of Tumor-Fibroblast Interactions Involved in Tumorigenicity. *PLoS Genet.* **2013**, *9(9)*, e1003789.
4. Shan, T.; Chen, S.; Chen, X.; Lin, W.R.; Li, W.; Ma, J.; Wu, T.; Cui, X.; Ji, H.; Li, Y.; Kang, Y. Cancer-Associated Fibroblasts Enhance Pancreatic Cancer Cell Invasion by Remodeling the Metabolic Conversion Mechanism. *Oncol. Rep.* **2017**, *37(4)*, 1971-1979.
5. Kim, S-H.; Choe, C.; Shin, Y-S.; Jeon, M-J.; Choi, S-J.; Lee, J.; Bae, G-Y.; Cha, H-J.; Kim, J. Human Lung Cancer-Associated Fibroblasts Enhance Motility of Non-Small Cell Lung Cancer Cells in Co-Culture. *Anticancer Res.* **2013**, *33(5)*, 2001-2009.
6. Metzler, V. M.; Pritz, C.; Riml, A.; Romani, A.; Tuertscher, R.; Steinbichler, T.; Dejaco, D.; Riechelmann, H.; Dudás, J. Separation of Cell Survival, Growth, Migration, and Mesenchymal Transdifferentiation Effects of Fibroblast Secretome on Tumor Cells of Head and Neck Squamous Cell Carcinoma. *Tumour Biol.* **2017**, *39(11)*, 1010428317705507.
7. Glenn, H. L.; Messner, J.; Meldrum, D. R. A Simple Non-Perturbing Cell Migration Assay Insensitive to Proliferation Effects. *Sci Rep-UK.* **2016**, *6(31694)*, 101038srep31694.


**www.agilent.com/lifesciences/biotek**




RA44169.1055671296





Printed in the USA, May 1, 2021
5994-2397EN


Agilent
Trusted Answers